

New Avenue for Accurate Analytical Waveforms and Fluxes for Eccentric Compact Binaries

Simone Albanesi^{1,2}, Andrea Placidi³, Alessandro Nagar^{2,4}, Marta Orselli^{3,5}, and Sebastiano Bernuzzi⁶

¹ *Dipartimento di Fisica, Università di Torino, via P. Giuria 1, 10125 Torino, Italy*

² *INFN Sezione di Torino, Via P. Giuria 1, 10125 Torino, Italy*

³ *Dipartimento di Fisica e Geologia, Università di Perugia,*

INFN Sezione di Perugia, Via A. Pascoli, 06123 Perugia, Italia

⁴ *Institut des Hautes Etudes Scientifiques, 91440 Bures-sur-Yvette, France*

⁵ *Niels Bohr Institute, Copenhagen University, Blegdamsvej 17, DK-2100 Copenhagen O, Denmark and*

⁶ *Theoretisch-Physikalisches Institut, Friedrich-Schiller-Universität Jena, 07743, Jena, Germany*

(Dated: September 1, 2022)

We introduce a new paradigm for constructing accurate analytic waveforms (and fluxes) for eccentric compact binaries. Our recipe builds on the standard Post-Newtonian (PN) approach but (i) retains implicit time-derivatives of the phase space variables in the instantaneous part of the noncircular waveform, and then (ii) suitably factorizes and resums this partly PN-implicit waveform using effective-one-body (EOB) procedures. We test our prescription against the exact results obtained by solving the Teukolsky equation with a test-mass source orbiting a Kerr black hole, and compare the use of the exact *vs* PN equations of motion for the time derivatives computation. Focusing only on the quadrupole contribution, we find that the use of the exact equations of motion yields an analytical/numerical agreement of the (averaged) angular momentum fluxes that is improved by 40% with respect to previous work, with 4.5% fractional difference for eccentricity $e = 0.9$ and black hole dimensionless spin $-0.9 \leq \hat{a} \leq +0.9$. We also find a remarkable convergence trend between Newtonian, 1PN and 2PN results. Our approach carries over to the comparable mass case using the resummed EOB equations of motion and paves the way to faithful EOB-based waveform model for long-inspiral eccentric binaries for current and future gravitational wave detectors.

I. INTRODUCTION

The accurate computation of the gravitational waves (GW) from eccentric compact binary mergers has recently prompted a vibrant activity by the analytical and numerical relativity community [1–18]. A main goal of this programme is to provide GW templates for binaries on generic orbits to be used in the next scientific observational runs of the LIGO-Virgo-Kagra (LVK) collaboration [19–21] and in the future LISA observations [22–24]. Indeed, LVK’s GW190521 event indicates that eccentricity might play a fundamental role for the analysis of stellar-mass binary black holes mergers [25–28]. Similarly, extreme-mass-ratio-inspirals (EMRIs) with eccentricity are expected to be detected by LISA [22–24],

The effective-one-body (EOB) approach to the two body problem [29–33], and in particular the `TEOBResumS` model [3, 4, 6, 34, 35], currently seems the only analytical framework close to delivering a quantitatively accurate model for arbitrary eccentricity, including dynamical captures. The model currently exhibits an acceptable level of flexibility and faithfulness with several exact results obtained numerically, from comparable mass binaries to extreme mass ratio inspirals [15, 16]. The model is also ready for parameter estimation, as shown for the case of GW190521 [27]. A central issue in the construction of eccentric EOB waveform models is the accurate analytical modelization of the radiation reaction force, i.e. the flux of energy and angular momentum emitted by the system that causes the orbit to shrink and circularize. Reference [3] introduced the eccentric `TEOBResumS` by dressing

the circular azimuthal component of the radiation reaction with the leading-order (Newtonian) noncircular contribution. The same idea is applied to the waveform [3]. Within this paradigm, several eccentric EOB models were constructed [3, 6, 7], so to support the analysis of GW190521 under the hyperbolic-capture hypothesis [27]. We note, however, that its quasi-circular limit is not as accurate as the native quasi-circular model [6, 7], still delivering unfaithfulnesses $< 3\%$ with Numerical Relativity (NR) waveform data. Building partly upon [13], the noncircular, factorized and resummed, EOB waveform was pushed to 2PN accuracy in [15]. Albanesi *et al.* [16] contrasted several proposal for the radiation reaction available in the literature and concluded that those based on the Newtonian-factorization (with a 2PN correction) deliver the most faithful representation of the fluxes of a test-mass around a Kerr black hole. Reference [15] used the 2PN-truncated equations of motion (EOM) to recast the noncircular correction in a simpler form, retaining explicit dependence on only the angular and radial momenta (P_φ, P_R). Unfortunately, with this approach the behavior at the orbit turning points (apastron and periastron) cannot be modified by higher PN corrections, since $P_R = 0$ there by definition and all noncircular corrections vanish. The accuracy at the radial turning points of the scheme is thus entirely determined by the Newtonian contribution, that explicitly depends on the, there nonvanishing, radial acceleration \ddot{R} , see [15, 16].

Here we propose a new strategy to significantly improve the behavior of the waveform at the radial turning points. The crucial element behind the accuracy of the generic Newtonian prefactor is that the derivatives

(and notably \ddot{R} , see Fig. 17 and 18 of [15]) are evaluated using the *exact* EOM and not the PN-truncated ones. This is the important keystone that allows one to increase the accuracy of Newtonian-like expressions in strong field (basically improving the Ruffini-Wheeler approximation [36], see also [37]). We extend here this idea to higher PN orders.

II. FROM THE MULTIPOLE MOMENTS TO THE FACTORIZED WAVEFORM

The multipolar decomposition of the strain waveform reads $h_+ - ih_\times = \mathcal{D}_L^{-1} \sum_{\ell=2}^{\infty} \sum_{m=-\ell}^{\ell} h_{\ell m} {}_{-2}Y_{\ell m}(\iota, \phi)$, where \mathcal{D}_L is the luminosity distance and ${}_{-2}Y_{\ell m}(\iota, \phi)$ the $s = -2$ spin-weighted spherical harmonics. Following Ref. [15], the multipolar eccentric waveform is written in factorized form as¹ $h_{\ell m} = h_{\ell m}^{(N,\epsilon)} \hat{h}_{\ell m}^c \hat{h}_{\ell m}^{\text{nc}}$, where:

- (i) $h_{\ell m}^{(N,\epsilon)}$ is the generic Newtonian prefactor, first used in Ref. [3] to extend the native quasi-circular **TEOBResumS** model to the eccentric case.
- (ii) $\hat{h}_{\ell m}^c$ is the PN circular correction, which is then further factorized and resummed following the most recent version of the procedure of Ref. [38], as now implemented in the quasi-circular **TEOBResumS** model [34, 35].
- (iii) $\hat{h}_{\ell m}^{\text{nc}}$ is the PN noncircular correction, formally introduced in Ref. [15]. This is further factorized in an hereditary contribution (or tail) and in an instantaneous part, $\hat{h}_{\ell m}^{\text{nc}} = \hat{h}_{\ell m}^{\text{nc,tail}} \hat{h}_{\ell m}^{\text{nc,inst}}$.

The computation of the noncircular factors of Ref. [15] employs as initial input the PN expanded spherical multipoles of the waveform of Refs. [13, 39]. Depending on the parity of the multipole, these are obtained from the corresponding mass-type (when $\ell + m$ is even) or current-type (when $\ell + m$ is odd) radiative spherical multipoles, respectively called $U_{\ell m}$ and $V_{\ell m}$,² which in turn are related to the symmetric trace-free (STF) source multipole moments by nonlinear PN relations involving time derivatives of the latter. In the case of the $\ell = m = 2$ mode, at 2PN one has³ $h_{22} = -U_{22}/(\sqrt{2}c^4)$, $U_{22} = 2\sqrt{3} \alpha_{22}^{ij} U_{ij}$, and $U_{ij} = \ddot{I}_{ij}$, where α_{22}^{ij} is one of the STF tensors which connect the basis of spherical harmonics to the STF one (see, e.g., Eq.(2.5) of Ref. [39] for their definition), U_{ij} is the STF radiative mass quadrupole, and I_{ij} is the STF mass quadrupole of the source. A standard intermediate step in this computation is to systematically replace

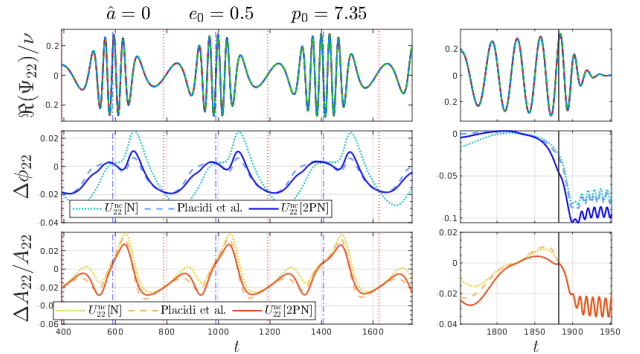


FIG. 1. Quadrupolar waveform generated by a test-mass plunging into a Schwarzschild black hole along an orbit with initial eccentricity $e_0 = 0.5$. Numerical waveform (black) compared to the EOB waveform with Newtonian noncircular corrections (red), to the one with 2PN noncircular corrections [15] (dashed green), and to the one proposed here (dash-dotted blue). Phase and relative amplitude differences are also shown.

the time derivatives of the dynamical variables, which stem from the time derivatives of the STF source moments, like \ddot{I}_{ij} , with the PN-expanded EOM. Here, we follow a different approach to obtain an alternative non-circular instantaneous factor where the time-derivatives are not replaced with the PN-expanded EOM. In practice: (i) we recover the 2PN accurate expressions for the STF source moments, valid for noncircular binaries, from Sec. IIIB of Ref. [39]; (ii) we trade the modified harmonic coordinates used therein for the EOB phase space variables $(r, \varphi, p_{r_*}, p_\varphi)$ ⁴ using the transformations given in Eqs. (5)–(8) of Ref. [15]; (iii) we build the radiative multipoles following Secs. II and IIIA of Ref. [39], by taking the needed time derivatives but *without* replacing them with the PN-expanded EOM; (iv) we factorize the Newtonian part, which is precisely $h_{\ell m}^{(N,\epsilon)}$; (v) we factorize the generic source term $\hat{S}_{\text{eff}}^{(\epsilon)}$, which corresponds to the mass-reduced EOB effective Hamiltonian \hat{H}_{eff} for even-parity multipoles and to the Newtonian-normalized angular momentum \hat{j}_φ for odd-parity multipoles; finally (vi) we factorize also the non-eccentric part of the residual, which is obtained by setting to zero p_{r_*} and all the time derivatives of the EOB dynamical variable except $\Omega \equiv \dot{\varphi}$. Note that this non-eccentric part *does not* coincide with the exact circular limit, as we will explain below. The $\ell = m = 2$ PN-expanded instantaneous contribution reads

$$h_{22}^{\text{inst}} = h_{22}^{(N,0)}(r, \dot{r}, \ddot{r}, \Omega, \dot{\Omega}) \quad (1)$$

¹ Following standard notation, the parity is $\epsilon = 0$ when $\ell + m$ is even and $\epsilon = 1$ when $\ell + m$ is odd.

² This separation takes place when the motion is planar, namely for spin-aligned configurations. In the general case for each multipole one needs both $U_{\ell m}$ and $V_{\ell m}$.

³ Throughout the paper we use dots to denote time derivatives.

⁴ In order of appearance $r \equiv R/M$ is the relative separation in the center of mass frame, φ is the orbital phase, $p_{r_*} \equiv (A/B)^{1/2} p_r$, where A, B are the 2PN accurate EOB potentials and $p_r \equiv P_R/\mu$ is the radial momentum, and $p_\varphi \equiv P_\varphi/\mu M$ is the angular momentum. Denoting with $m_{1,2}$ the individual masses of the binary we have $M \equiv m_1 + m_2$, $\mu \equiv m_1 m_2 / M$ and $q \equiv m_1 / m_2 \geq 1$.

$$\begin{aligned}
& + \frac{1}{c^2} h_{22}^{(1\text{PN},0)}(r, \dot{r}, \ddot{r}, \Omega, \dot{\Omega}, p_{r_*}, \dot{p}_{r_*}, \ddot{p}_{r_*}, p_\varphi, \dot{p}_\varphi, \ddot{p}_\varphi) \\
& + \frac{1}{c^4} h_{22}^{(2\text{PN},0)}(r, \dot{r}, \ddot{r}, \Omega, \dot{\Omega}, p_{r_*}, \dot{p}_{r_*}, \ddot{p}_{r_*}, p_\varphi, \dot{p}_\varphi, \ddot{p}_\varphi),
\end{aligned}$$

where and $h_{22}^{(N,0)}$ is the Newtonian part and $(h_{22}^{(1\text{PN},0)}, h_{22}^{(2\text{PN},0)})$ formally addresses the contributions obtained by taking the time-derivative of the corresponding terms in the radiative multipoles while keeping all derivatives explicit. We obtain

$$\begin{aligned}
h_{22}^{(N,0)} &\equiv -8\sqrt{\frac{\pi}{5}}\nu r^2\Omega^2 e^{-2i\varphi} \hat{h}_{22}^{(N,0)\text{nc}}, \quad (2) \\
\hat{h}_{22}^{(N,0)\text{nc}} &= 1 - \frac{1}{2} \left(\frac{\dot{r}^2}{r^2\Omega^2} + \frac{\ddot{r}}{r\Omega^2} \right) + i \left(\frac{2\dot{r}}{r\Omega} + \frac{\dot{\Omega}}{2\Omega^2} \right),
\end{aligned}$$

with the noncircular part $\hat{h}_{22}^{(N,0)\text{nc}}$ isolated. The non-circular contribution is obtained from Eq. 1 as follows. First, we define the instantaneous, total, factorized correction as $f_{22}^{\text{total}} \equiv h_{22}^{\text{inst}} \left(h_{22}^{(N,0)} \hat{H}_{\text{eff}} \right)^{-1}$, where we replaced $\hat{S}_{\text{eff}}^{(0)} \equiv \hat{H}_{\text{eff}}$. The non-eccentric limit of this function is defined according to point (iv) above, so to obtain (at 2PN)

$$\begin{aligned}
f_{22}^{\text{circ}} &= 1 + \frac{u}{c^2} \left[-\frac{12}{7} - \frac{p_\varphi^2 u}{3} + \left(\frac{1}{7} + \frac{p_\varphi^2 u}{2} \right) \nu \right] \\
&+ \frac{u^2}{c^4} \left[-\frac{229}{252} - \frac{929p_\varphi^2 u}{756} + \frac{19p_\varphi^4 u^2}{63} \right. \\
&+ \left. \left(\frac{289}{126} - \frac{1741p_\varphi^2 u}{378} - \frac{235p_\varphi^4 u^2}{504} \right) \nu \right. \\
&+ \left. \left(\frac{65}{126} + \frac{31p_\varphi^2 u}{54} - \frac{143p_\varphi^4 u^2}{504} \right) \nu^2 \right]. \quad (3)
\end{aligned}$$

Note that p_φ is *not* replaced with its PN-expanded circular expression. The noncircular (instantaneous) contribution is obtained factoring out this result as $\hat{h}_{22}^{\text{ncinst}} = T_{2\text{PN}} [f_{22}^{\text{total}}(f_{22}^{\text{circ}})^{-1}]$, where $T_{2\text{PN}}$ indicates an expansion up to the 2PN order. This allows us to obtain a new non-circular factor that is analogous, though different, to that of Ref. [15]. A few more comments are in order to further clarify the structure of the non-eccentric (i.e. circular) part. First, we stress that taking the exact *circular limit* of the product $h_{22}^{(N,0)} f_{22}^{\text{circ}}$ (i.e., replacing also the PN-expanded expression of p_φ along circular orbits) correctly delivers the 2PN-accurate f_{22} function of Eq. (B1) of Ref. [38]. The factorization procedure is thus such that the waveform is consistent with the quasi-circular waveform of `TEOBResumS`⁵. We note, however, that in

⁵ In Ref. [15] we factorized the *circular* $\hat{S}_{\text{eff}}^{(\epsilon)}$, but the procedure followed in this work is more consistent since in the full EOB waveform we have the generic factor $\hat{S}_{\text{eff}}^{(\epsilon)}$, see e.g. Ref. [38].

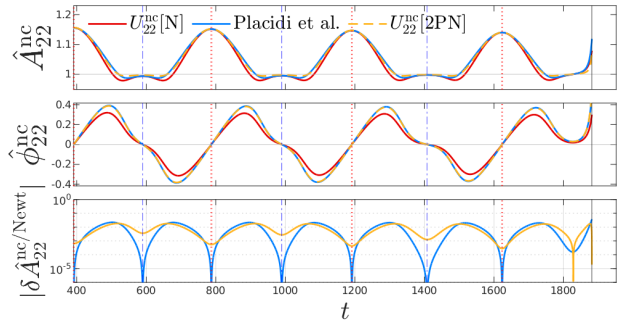


FIG. 2. Same configuration of Fig. 1: comparing the 2PN-accurate instantaneous noncircular correction to the amplitude (top) and to the phase (middle) of this work with the one of Placidi et al.[15]. Bottom: relative difference with the Newtonian contribution. The noncircular factor introduced here is nonzero at the apastron (red dotted vertical lines) and periastron (blue dash-dotted vertical lines). The black vertical line marks the merger time.

practice we *do not* use the 2PN-accurate f_{22}^{circ} recovered above, but rather replace it with the quasi-circular function $\rho_{22} = f_{22}^{1/2}$ with the PN-accuracy and resummation used either in the standard `TEOBResumS` model (for comparable masses) or in its test-mass version [8]. More precisely, ρ_{22} is resummed according to Refs. [40, 41], but while in `TEOBResumS` the orbital contribution ρ_{22}^{orb} is Taylor-expanded at 3⁺PN accuracy [42], in the test-mass limit we use it at 6PN, resummed with a (4,2) Padé approximant.

The new noncircular factor is given explicitly in a supplemental `Mathematica` notebook. The noncircular tail contribution $\hat{h}_{\ell m}^{\text{nc,tail}}$ is resummed following Ref. [15], while the circular tail contributions are incorporated according to standard procedure [38]. From the waveform, the quadrupolar fluxes read [43] $\dot{E}_{22} = \frac{1}{8\pi} |\dot{h}_{22}|^2$ and

$$\dot{J}_{22} = -\frac{1}{4\pi} \Im \left(\dot{h}_{22} h_{22}^* \right).$$

III. COMPARING ANALYTICAL AND NUMERICAL RESULTS

The new prescription for the noncircular waveform correction is tested by following step-by-step the approach of Ref. [8, 15, 16]. This relies on extensive comparisons with waveform and fluxes emitted by a (nonspinning) particle orbiting around a Kerr black hole, considering various orbital configurations. To set the stage, we consider a particle inspiralling and plunging around a Schwarzschild black hole and compare the analytical waveform with the numerical one, considered exact, obtained solving numerically the Teukolsky equation using `Teukode` [44] (see Ref. [8] for more numerical details). Figure 1 refers to a configuration with initial eccentricity $e_0 = 0.5$ and semilatus rectum $p_0 = 7.35$. The numerical waveform (black) is compared with the analytical waveform with

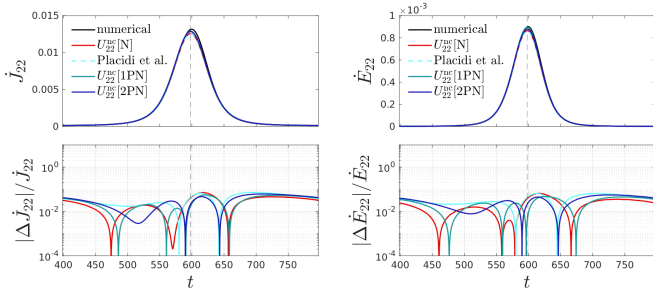


FIG. 3. Angular momentum and energy quadrupolar fluxes at infinity generated by a test-particle in Schwarzschild space-time along a geodesic with $e = 0.5$ and $p = 9$. The relative differences in the bottom panels show that the the PN waveform corrections with explicit derivatives improve the analytical/numerical agreement at periastron.

Newtonian noncircular corrections (red), the waveform with 2PN noncircular corrections proposed in Ref. [15] (dashed green), and the waveform with 2PN noncircular corrections as proposed in this work (blue dash-dotted). The derivatives of coordinates and momenta which appear in the noncircular corrections are computed numerically with a 4th-order centered-stencil scheme. The corresponding analytical/numerical differences for amplitude and phase are shown in the bottom panels. Regarding the phase, the performance of the new waveform and of the one of Ref. [15] are substantially equivalent (see the dashed and solid blue lines in the middle panel of Fig. 1). For the amplitude, instead, the new approach yields a reduced maximum analytical/numerical difference during the evolution, as well as a slight improvement as the orbital motion approaches the periastra (see bottom panel of Fig. 1). This comes from the nonvanishing of the noncircular correction at the radial turning point. This is highlighted in Fig. 2, which shows the noncircular corrections corresponding to Fig. 1. The bottom panel exhibits the relative difference between the two 2PN noncircular amplitude corrections and the Newtonian noncircular amplitude correction, $|\delta \hat{A}_{22}^{\text{nc/Newt}}|$. The correction at the two turning points is nonzero and is especially relevant at periastron. Note that the *instantaneous* phase noncircular corrections at 2PN differ sensibly from the Newtonian one. However, part of this difference is compensated by the hereditary phase correction, as already highlighted in Sec. IIIC of Ref. [15].

The improvement in the description of the waveform at periastron is even more important when the noncircular corrections are incorporated in the fluxes. Note in fact that the main contribution to the dynamics, through radiation reaction, happens due to the burst of radiation emitted at periastron. To show this effect systematically, we consider a set of geodesic eccentric orbits with dimensionless Kerr spin $|\hat{a}| \leq 0.9$, eccentricity up to $e = 0.9$ and semilata recta given by $p = p_{\text{schw}} p_s(e, \hat{a}) / p_s(e, 0)$, where p_s is the separatrix [45, 46] and $p_{\text{schw}} = (9, 13)$. The definitions of eccentricity and semilata rectum used

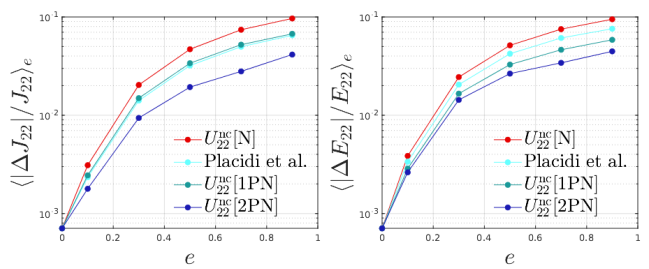


FIG. 4. Analytical/numerical fractional differences between the averaged quadrupolar fluxes versus eccentricity that show convergence of PN corrections in the test-mass limit. Each point is obtained from the mean of the orbital averaged fluxes of all the configurations considered at a given eccentricity e . See the main text for more details.

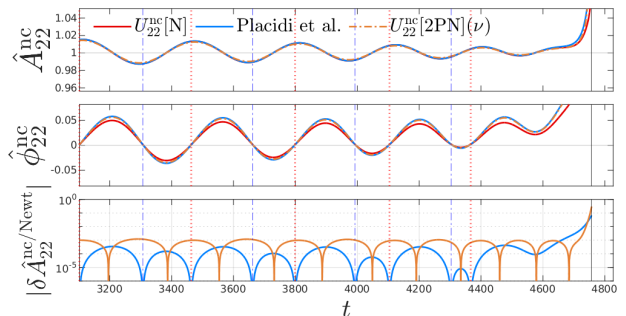


FIG. 5. Same scheme as Fig. 2, but for an eccentric inspiral binary with $e_0 = 0.07621$ and $q = 1.22$ obtained with the full EOB dynamics of [15].

here can be found in Ref. [8], together with more details on the numerical data. In Fig. 3 we compare the fluxes for a case example with $e = 0.5$. From the analytical/numerical relative differences one finds that the 2PN noncircular corrections with explicit derivatives perform better at periastron. As radiation reaction, these fluxes will drive faster inspirals than those driven by the simple leading (Newtonian) noncircular correction of [8]. To draw a more global picture, it is useful to compare the orbital-averaged analytical fluxes with the corresponding, averaged, numerical ones obtained from the exact waveforms, calculated solving the Teukolsky equation. We compute the analytical/numerical relative difference and for each value of eccentricity e we compute its average over all the dataset sharing the same value of e . These averages are shown in Fig. 4, where each point has been obtained by averaging the analytical/numerical relative differences of 14 simulations with $\hat{a} = (0, \pm 0.2, \pm 0.6, \pm 0.9)$ and two different values of p . As shown in Fig. 4, the new 2PN waveform yields (on average) the best analytical/numerical agreement; even the 1PN energy flux calculation is better than the 2PN-accurate expression of Ref. [15]. Note however that the average over all spinning configurations can hide some information. In particular, for highly eccentric configurations ($e = 0.9$), the Newtonian prescription yields a better analytical/numerical

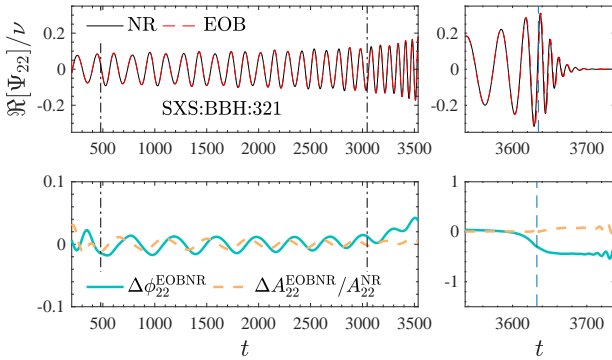


FIG. 6. Illustrative EOB/NR phasing comparison with the NR dataset SXS:BBH:321 of the SXS catalog [47]. The EOB/NR phase difference is reduced during the plunge with respect to the corresponding plot in Fig. 13 of Ref. [15]. The noncircular waveform correction is shown in Fig. 5.

agreement when averaged only on negative spins. This is clearer for the lowest spin, $\hat{a} = -0.9$, since the Newtonian flux yields a better analytical/numerical agreement even for mild eccentricities ($e \gtrsim 0.3$). However, in the Schwarzschild case, the hierarchy of the different prescriptions is the same shown in Fig. 4.

The new noncircular correction factor is quantitatively superior to all other previous attempts of incorporating high PN noncircular information in the waveform and fluxes. This is further corroborated by the following: the instantaneous amplitude correction presented in Eq. (37) of Ref. [15] contains a 1PN term $\propto -p_{T_*}^2 r$, that can become extremely large when considering hyperbolic or eccentric orbits with large radius. While this issue is not relevant for any of the configurations considered in Ref. [15], the correction can become even negative, and thus unphysical, for large separations, e.g. those occurring in hyperbolic encounters. By contrast, the new waveform is well-behaved *also* for a hyperbolic encounter or scattering configuration starting from any, arbitrarily large, initial separation.

The same behavior carries over to the comparable-mass case, with the test-mass dynamics replaced by the resummed EOB dynamics. Figure 5 exhibits the time-evolution of the noncircular waveform corrections along the EOB dynamics of a binary corresponding to the NR configuration SXS:BBH:321 of the SXS catalog [47], row #23 in Table IV of Ref. [15]. In this case, the mass ratio is $q = 1.22$, while the dimensionless spins (χ_1, χ_2), aligned with the orbital angular momentum, are $\chi_1 = +0.33$ and $\chi_2 = -0.44$. The initial EOB eccentricity at the apastron is small, $e_{\omega_a}^{\text{EOB}} = 0.07621$, but large enough to probe that our new waveform brings an improvement with respect to previous work. First of all, Fig. 5 indicates that in the comparable-mass case the amplitude correction at the radial turning points is more relevant than in the test-mass case (cf. Fig. 2), although the correction is small. It is informative to look at a standard EOB/NR phasing comparison for SXS:BBH:321, that we

report in Fig. 6. The EOB waveform is aligned to the NR one by minimizing the phase difference in the frequency interval corresponding to the two vertical lines in the left panels of the figure. The top panels compare the EOB and NR real parts of the waveform, while the bottom panels show the EOB/NR phase difference $\Delta\phi_{22}^{\text{EOBNR}} \equiv \phi_{22}^{\text{EOB}} - \phi_{22}^{\text{NR}}$ and relative amplitude difference, with $\Delta A_{22}^{\text{EOBNR}} \equiv A_{22}^{\text{EOB}} - A_{22}^{\text{NR}}$. The picture illustrates that $\Delta\phi_{22}^{\text{EOBNR}}$ is reduced, during the late-inspiral and plunge, with respect to the corresponding plot in Fig. 13 of Ref. [15], with the same waveform alignment interval used here. A similar behavior is also found with higher eccentricities. However, it must be noted that since the waveform is different, the choice of the initial parameters, which is not changed in this case, possibly might be optimized further. This study, together with the analysis of higher modes, is postponed to future work.

We finally point out that the waveform differences due to the new noncircular correction will yield fluxes which are *larger* at apastron than the current ones. Once recasted in the form of radiation reaction force, and incorporated within the EOB dynamics, the new prescription will eventually yield an additional acceleration of the eccentric inspiral due to the stronger emission at periastron. The development of the radiation reaction force and its influence on the inspiral (for any mass ratio) is also deferred to future work. To do so, we will use, and generalize, the approach adopted for the generic Newtonian prefactor [3]. This calculation relies on the iterative procedure for computing the time-derivatives including dissipative terms, see Appendix A of Ref. [48].

IV. CONCLUSION

We introduced a new way of exploiting PN results for the waveform emitted by eccentric and hyperbolic binaries. The key idea is to use the full, resummed EOB EOM to compute the time derivatives in the formal expression of the analytical waveform, rather than replacing them with the PN-expanded EOM. This exploits the robust behavior of the EOB model in the strong-field regime. This procedure effectively generalizes the use of the generic Newtonian prefactor to higher PN orders. We comprehensively tested this approach against a large set of data for waveforms and fluxes emitted by a test-mass orbiting a Kerr black hole and we showed that these findings carry over to the comparable mass case. The novel use of PN results, within the EOB framework, yields considerable improvement in the waveform accuracy. Typically, one starts from PN-expanded results and then devise specific techniques to improve their behavior in strong field. Our findings indicate that this is not sufficient, but it is actually possible to do better by removing some of the intermediate steps involving PN-expansions. In particular, our approach does not rely on eccentricity-expanded fluxes, in contrast to [49, 50], and remains robust also for highly eccentric configurations.

ACKNOWLEDGMENTS

We are indebted to P. Rettegno for a crucial check on the 2PN waveform of Ref. [15] that eventually prompted this study. We are grateful to C. Munna for informative discussions and explanations about his PN results. We also thank Tony Garbato for continuous support dur-

ing the development of this work. S.B. acknowledges support by the EU H2020 under ERC Starting Grant, no. BinGraSp-714626. M.O. and A.P. acknowledge support from the project ‘‘MOSAICO’’ financed by Fondo Ricerca di Base 2020 of the University of Perugia. M.O. and A.P. thank the Niels Bohr Institute for hospitality. Computations were performed on the ‘‘Tullio’’ server in Torino, supported by INFN.

-
- [1] I. Hinder, L. E. Kidder, and H. P. Pfeiffer, (2017), arXiv:1709.02007 [gr-qc].
- [2] T. Hinderer and S. Babak, Phys. Rev. **D96**, 104048 (2017), arXiv:1707.08426 [gr-qc].
- [3] D. Chiaramello and A. Nagar, Phys. Rev. D **101**, 101501 (2020), arXiv:2001.11736 [gr-qc].
- [4] A. Nagar, P. Rettegno, R. Gamba, and S. Bernuzzi, Phys. Rev. D **103**, 064013 (2021), arXiv:2009.12857 [gr-qc].
- [5] T. Islam, V. Varma, J. Lodman, S. E. Field, G. Khanna, M. A. Scheel, H. P. Pfeiffer, D. Gerosa, and L. E. Kidder, (2021), arXiv:2101.11798 [gr-qc].
- [6] A. Nagar, A. Bonino, and P. Rettegno, Phys. Rev. D **103**, 104021 (2021), arXiv:2101.08624 [gr-qc].
- [7] A. Nagar and P. Rettegno, (2021), arXiv:2108.02043 [gr-qc].
- [8] S. Albanesi, A. Nagar, and S. Bernuzzi, Phys. Rev. D **104**, 024067 (2021), arXiv:2104.10559 [gr-qc].
- [9] X. Liu, Z. Cao, and Z.-H. Zhu, (2021), arXiv:2102.08614 [gr-qc].
- [10] Q. Yun, W.-B. Han, X. Zhong, and C. A. Benavides-Gallego, Phys. Rev. D **103**, 124053 (2021), arXiv:2104.03789 [gr-qc].
- [11] A. Tucker and C. M. Will, Phys. Rev. D **104**, 104023 (2021), arXiv:2108.12210 [gr-qc].
- [12] Y. Setyawati and F. Ohme, Phys. Rev. D **103**, 124011 (2021), arXiv:2101.11033 [gr-qc].
- [13] M. Khalil, A. Buonanno, J. Steinhoff, and J. Vines, Phys. Rev. D **104**, 024046 (2021), arXiv:2104.11705 [gr-qc].
- [14] A. Ramos-Buades, A. Buonanno, M. Khalil, and S. Ossokine, Phys. Rev. D **105**, 044035 (2022), arXiv:2112.06952 [gr-qc].
- [15] A. Placidi, S. Albanesi, A. Nagar, M. Orselli, S. Bernuzzi, and G. Grignani, Phys. Rev. D **105**, 104030 (2022), arXiv:2112.05448 [gr-qc].
- [16] S. Albanesi, A. Nagar, S. Bernuzzi, A. Placidi, and M. Orselli, Phys. Rev. D **105**, 104031 (2022), arXiv:2202.10063 [gr-qc].
- [17] S. R. Chowdhury and M. Khlopov, Symmetry **14**, 510 (2022), arXiv:2203.00507 [gr-qc].
- [18] P. Saini, M. Favata, and K. G. Arun, (2022), arXiv:2203.04634 [gr-qc].
- [19] R. Abbott *et al.* (LIGO Scientific, VIRGO, KAGRA), (2021), arXiv:2111.03606 [gr-qc].
- [20] R. Abbott *et al.* (LIGO Scientific, VIRGO, KAGRA), (2022), arXiv:2203.01270 [gr-qc].
- [21] H. Abe *et al.* (KAGRA), (2022), arXiv:2203.07011 [astro-ph.IM].
- [22] P. Amaro-Seoane *et al.* (LISA), (2017), arXiv:1702.00786 [astro-ph.IM].
- [23] S. Babak, J. Gair, A. Sesana, E. Barausse, C. F. Sopuerta, C. P. L. Berry, E. Berti, P. Amaro-Seoane, A. Petiteau, and A. Klein, Phys. Rev. D **95**, 103012 (2017), arXiv:1703.09722 [gr-qc].
- [24] J. R. Gair, S. Babak, A. Sesana, P. Amaro-Seoane, E. Barausse, C. P. L. Berry, E. Berti, and C. Sopuerta, J. Phys. Conf. Ser. **840**, 012021 (2017), arXiv:1704.00009 [astro-ph.GA].
- [25] R. Abbott *et al.* (LIGO Scientific, Virgo), Phys. Rev. Lett. **125**, 101102 (2020), arXiv:2009.01075 [gr-qc].
- [26] V. Gayathri, J. Healy, J. Lange, B. O’Brien, M. Szczepanczyk, I. Bartos, M. Campanelli, S. Klimentko, C. O. Lousto, and R. O’Shaughnessy, Nature Astron. **6**, 344 (2022), arXiv:2009.05461 [astro-ph.HE].
- [27] R. Gamba, M. Breschi, G. Carullo, P. Rettegno, S. Albanesi, S. Bernuzzi, and A. Nagar, Submitted to Nature Astronomy (2021), arXiv:2106.05575 [gr-qc].
- [28] I. M. Romero-Shaw, P. D. Lasky, and E. Thrane, Astrophys. J. Lett. **921**, L31 (2021), arXiv:2108.01284 [astro-ph.HE].
- [29] A. Buonanno and T. Damour, Phys. Rev. **D59**, 084006 (1999), arXiv:gr-qc/9811091.
- [30] A. Buonanno and T. Damour, Phys. Rev. **D62**, 064015 (2000), arXiv:gr-qc/0001013.
- [31] T. Damour, P. Jaranowski, and G. Schaefer, Phys. Rev. **D62**, 084011 (2000), arXiv:gr-qc/0005034 [gr-qc].
- [32] T. Damour, Phys. Rev. **D64**, 124013 (2001), arXiv:gr-qc/0103018.
- [33] T. Damour, P. Jaranowski, and G. Schäfer, Phys. Rev. **D91**, 084024 (2015), arXiv:1502.07245 [gr-qc].
- [34] A. Nagar, G. Riemenschneider, G. Pratten, P. Rettegno, and F. Messina, Phys. Rev. D **102**, 024077 (2020), arXiv:2001.09082 [gr-qc].
- [35] G. Riemenschneider, P. Rettegno, M. Breschi, A. Albertini, R. Gamba, S. Bernuzzi, and A. Nagar, Phys. Rev. D **104**, 104045 (2021), arXiv:2104.07533 [gr-qc].
- [36] R. Ruffini and J. A. Wheeler, in *Atti del convegno internazionale sul tema: The astrophysical aspects of weak interactions. Cortona, il Palazzone, 10-12 giugno 1970*, Vol. 157, edited by L. Radicati (Accademia Nazionale dei Lincei, Rome, 1971) p. 165.
- [37] A. Nagar, T. Damour, and A. Tartaglia, Class. Quant. Grav. **24**, S109 (2007), arXiv:gr-qc/0612096.
- [38] T. Damour, B. R. Iyer, and A. Nagar, Phys. Rev. **D79**, 064004 (2009), arXiv:0811.2069 [gr-qc].
- [39] C. K. Mishra, K. G. Arun, and B. R. Iyer, Phys. Rev. **D91**, 084040 (2015), arXiv:1501.07096 [gr-qc].
- [40] A. Nagar and A. Shah, Phys. Rev. **D94**, 104017 (2016), arXiv:1606.00207 [gr-qc].
- [41] F. Messina, A. Maldarella, and A. Nagar, Phys. Rev. **D97**, 084016 (2018), arXiv:1801.02366 [gr-qc].

- [42] T. Damour and A. Nagar, Phys. Rev. **D79**, 081503 (2009), arXiv:0902.0136 [gr-qc].
- [43] A. Nagar and L. Rezzolla, Class. Quant. Grav. **22**, R167 (2005), arXiv:gr-qc/0502064.
- [44] E. Harms, S. Bernuzzi, A. Nagar, and A. Zenginoglu, Class.Quant.Grav. **31**, 245004 (2014), arXiv:1406.5983 [gr-qc].
- [45] R. W. O’Shaughnessy, Phys. Rev. D **67**, 044004 (2003), arXiv:gr-qc/0211023.
- [46] L. C. Stein and N. Warburton, Phys. Rev. D **101**, 064007 (2020), arXiv:1912.07609 [gr-qc].
- [47] “SXS Gravitational Waveform Database,” <https://data.black-holes.org/waveforms/index.html>.
- [48] T. Damour, A. Nagar, and S. Bernuzzi, Phys.Rev. **D87**, 084035 (2013), arXiv:1212.4357 [gr-qc].
- [49] C. Munna, C. R. Evans, S. Hopper, and E. Forseth, Phys. Rev. D **102**, 024047 (2020), arXiv:2005.03044 [gr-qc].
- [50] C. Munna, Phys. Rev. D **102**, 124001 (2020), arXiv:2008.10622 [gr-qc].